Research on Engineering Structures & Materials
www.jresm.org
Research Group

Research Article

Bond behavior of deformed steel bars in fly ash–based geopolymer concrete: Test results and development-length implications

Tran Viet Hung*,a

Faculty of Civil Engineering, University of Transport and Communications, Hanoi, Vietnam

Article Info

Article History:

Received 23 Feb 2026

Accepted 29 May 2026

Keywords:

Geopolymer concrete;
Fly ash;
Bond–slip;
Pull-out test

Abstract

Fly ash geopolymer concrete (GPC) is a low-carbon alternative to Portland cement concrete. A reliable bond between steel reinforcement and GPC is essential for structural design. This study investigates the bond behavior of deformed steel bars embedded in fly ash GPC. The GPC mixtures are activated with a sodium hydroxide–sodium silicate solution and heat-cured at 60 °C for 24 h. Pull-out tests are conducted to obtain bond stress–slip curves. The peak bond stress, the slip at peak, and the residual bond stress are reported. The influence of compressive strength and confinement conditions is examined. The test results are compared with common bond models developed for Portland cement concrete. The comparisons show systematic differences in peak bond and post-peak softening. A simple calibration is proposed to adapt existing models for fly ash GPC. The calibrated model is used to discuss development-length implications for reinforced GPC members.

1. Introduction

Concrete remains the most widely used structural material, but recent development is increasingly driven by decarbonization, durability, and performance-based design. As research expands from conventional OPC concrete to low-carbon binders (including geopolymer/alkali-activated systems) and high-performance matrices such as UHPC, there is a growing need to reassess bond and anchorage behavior beyond OPC-based assumptions [1,2]. In particular, changes in matrix composition and cracking response may alter bond stress transfer and splitting sensitivity, which motivates the present investigation on fly ash-based geopolymer concrete (GPC) [3,4]. GPC is a promising low-carbon alternative to ordinary Portland cement concrete (OPC) [5-7]. GPC replaces Portland clinker with an aluminosilicate precursor that is activated by alkaline solutions. It can reduce embodied CO_2 and can valorize industrial by-products [8]. It can also achieve compressive strengths that are suitable for structural applications [9]. These advantages support increasing interest in using GPC in reinforced concrete members [10-12].

Structural use of GPC requires reliable design information [13,14]. The bond between deformed steel bars and the surrounding concrete is a governing mechanism. Bond controls govern the transfer of load from steel to concrete. Bond also controls crack spacing and crack width. Bond determines development length and lap splice length. Bond affects stiffness and rotation capacity in flexural members. A reinforced member can be unsafe if bond demand exceeds bond capacity. A reinforced member can be uneconomical if the development length is overestimated [15].

Bond in OPC concrete is well studied [16,17]. Bond resistance is commonly described by a bond stress–slip relationship. The relationship reflects adhesion, friction, and mechanical interlock of

*Corresponding author: hungtv@utc.edu.vn
[a]orcid.org/0000-0003-2614-7273
DOI: http://dx.doi.org/10.17515/resm2026-1528me0223rs

ribs. The relationship depends on concrete strength and cover. The relationship depends on bar diameter and bar surface geometry. The relationship depends on confinement from transverse reinforcement or external pressure. The relationship also depends on casting position and local bleeding effects. Bond failure in OPC concrete is typically classified as pull-out failure or splitting failure [18]. Pull-out failure occurs when ribs crush the surrounding concrete and the bar is extracted with limited radial cracking. Splitting failure occurs when radial stresses induce longitudinal cracks, leading to cover separation [19]. Splitting failure is common when the cover is small or the confinement is weak. Many design codes embed this knowledge through empirical rules and simplified bond models [20]. Several widely used analytical bond laws and code expressions were calibrated on OPC concrete databases [21,22]. These models are widely adopted for development length and lap splice provisions. They also support nonlinear analysis via τ–s laws and tension-stiffening models.

The direct use of OPC-based bond models for GPC is not necessarily justified [23]. GPC differs from OPC concrete in binder chemistry and microstructure. GPC often exhibits a different elastic modulus at a given compressive strength. GPC can show different pre-peak nonlinearity and post-peak softening in compression. GPC can also exhibit different interfacial transition zones and pore structures, depending on precursor type, activator composition, and curing regime. These differences can influence rib bearing, concrete crushing around ribs, and splitting resistance. The failure mode can shift with curing and mixture design. The post-peak bond response can also change due to different fracture processes and different stiffness of the surrounding matrix.

Published studies on bond in geopolymer and alkali-activated concretes show mixed trends [24], [25,26]. Some studies report peak bond stress comparable to or higher than OPC at similar compressive strength [27,28]. Some studies report lower bond capacity under certain curing regimes or for specific precursors. Many results show that confinement strongly influences the failure mode in GPC, as it does in OPC. Several studies indicate that post-peak softening and residual bond stress can differ from OPC [29,30]. However, the available evidence remains fragmented. Many studies use different precursors and different activators. Many studies use different curing temperatures and durations. Many studies use different specimen geometries and embedment lengths. They report only peak bond stress without full τ–s curves. Many studies do not provide sufficient information for design calibration. As a result, there is no widely accepted bond model for fly ash–based GPC that can be used with confidence in reinforced concrete design [31,32].

This gap is relevant for practical implementation. Fly ash–based GPC commonly requires heat curing to achieve stable strength development in many formulations [33]. Heat curing can densify the matrix and can modify early-age cracking behavior. Heat curing can also influence shrinkage and microcracking near the steel interface. These effects can directly influence bond and splitting resistance. Design provisions for anchorage and splicing typically assume OPC-based behavior. A systematic bias in bond capacity would translate into a systematic bias in development length. This bias can be unconservative if the bond is overestimated. This bias can also be overly conservative if the bond is underestimated. Both outcomes are undesirable. Unconservative design threatens safety. Overly conservative design penalizes material adoption and increases reinforcement congestion.

A focused experimental dataset is therefore needed. The dataset should target a well-defined material system. The system should use fly ash as the precursor. The system should use a sodium hydroxide–sodium silicate activator, which is common in practice. The system should employ a curing regime that is typical for fly ash GPC. The dataset should cover a practical strength range for structural applications. The dataset should include full bond stress–slip curves. The dataset should document failure modes. The dataset should also allow comparison against conventional OPC-based bond models and code expressions.

This paper addresses these needs. The study investigates the bond behavior of deformed steel bars embedded in fly ash–based geopolymer concrete [34]. The geopolymer mixtures are activated by a sodium hydroxide–sodium silicate solution. The specimens are heat-cured under a controlled temperature regime. Pull-out tests are performed to obtain complete bond stress–slip curves. The study reports peak bond stress and slip at peak. The study reports residual bond stress at larger

slips. The study classifies failure modes as pull-out or splitting. The study examines the influence of compressive strength and confinement conditions, as permitted by the test matrix. The study then compares the measured bond response with representative bond models that were originally developed for OPC concrete. The comparison focuses on peak bond capacity and post-peak softening characteristics. The study finally proposes a simple calibration approach. The approach adapts an existing OPC-based bond model to fly ash GPC through a small number of parameters. The calibrated model is then used to discuss development-length implications for reinforced fly ash GPC members.

2. Experimental Program

2.1. Materials and Mixture Design

This study used low-calcium fly ash to produce fly ash–based geopolymer concrete (GPC). The fly ash was obtained from Pha Lai thermal power plant (Vietnam). The fly ash satisfied the requirements for Class F fly ash. Its chemical composition is summarized in Table 1. The main oxide components were SiO_2, Al_2O_3, and Fe_2O_3, while the CaO content was low, which is consistent with the classification of the material as a low-calcium Class F fly ash [35]

Table 1. Chemical composition of the fly ash used in this study

Component	Content (mass %)
SiO_2	51.74
Al_2O_3	24.53
Fe_2O_3	5.59
CaO	0.81
Loss on ignition (LOI)	8.98

The alkaline activator consisted of sodium hydroxide (NaOH) and sodium silicate (Na_2SiO_3). The main properties of the activator components are summarized in Table 2. Solid NaOH flakes with a purity of 98% were dissolved in water to prepare solutions with target molarities of 12 M, 14 M, and 16 M. The sodium silicate solution had a silicate modulus of SiO_2/Na_2O = 2.5. The mass ratio Na_2SiO_3/NaOH was kept constant at 2.5 for all mixtures

Table 2. Main properties of the alkaline activator used in this study

Component	Parameter	Value
NaOH flakes	Purity	98%
NaOH solution	Target molarity	12 M, 14 M, 16 M
NaOH solution	NaOH required for 1 kg of solution	361 g (12 M), 404 g (14 M), 444 g (16 M)
Na_2SiO_3 solution	Silicate modulus, SiO_2/Na_2O	2.5
Na_2SiO_3 solution	Na_2O content (mass %)	11.8
Na_2SiO_3 solution	SiO_2 content (mass %)	29.5
Na_2SiO_3 solution	Water content (mass %)	58.7
Combined activator	Na_2SiO_3/NaOH mass ratio	2.5

A conventional aggregate skeleton was adopted. The aggregate content was selected to be comparable to ordinary concrete. The target fresh unit weight was 2400 kg/m^3. The total aggregate mass was taken as 1848 kg/m^3. Fine aggregate was set to 30% of the total aggregate mass. The sand content was therefore 554.4 kg/m^3. Mixture design focused on two key parameters. The first parameter was NaOH molarity (M). The second parameter was the activator-to-fly ash mass ratio (AAS/FA). The investigated range of AAS/FA was 0.40–0.50. The ratio was selected because the aggregates were used in a dry condition. Lower ratios produced mixtures that were too stiff for mixing and casting. Three mixtures were selected for structural-strength levels. The mixtures targeted nominal compressive strengths of 30, 40, and 50 MPa. The mixtures are denoted as G30, G40, and G50. Na_2SiO_3/NaOH was fixed at 2.5. NaOH molarity was 12 M, 14 M, and 16 M for G30,

G40, and G50, respectively. All specimens were heat cured at 60 °C for 24 h. The mixture proportions for the three GPC mixtures (G30, G40, and G50) are summarized in Table 3.

Table 3. Mixture proportions of fly ash–based GPC (kg/m^3)

Component	G30	G40	G50
Fly ash	372.52	375.84	390.35
Fine aggregate (sand)	554.0	554.0	554.0
Coarse aggregate 2.36–4.75 mm	64.68	64.68	64.68
Coarse aggregate 4.75–9.50 mm	420.42	420.42	420.42
Coarse aggregate 9.50–19.0 mm	743.82	743.82	743.82
Coarse aggregate 19.0–25.0 mm	65.68	65.68	65.68
NaOH solution	51.28 (12 M)	50.33 (14 M)	46.18 (16 M)
Na_2SiO_3 solution	128.20	125.83	115.46
Na_2SiO_3/NaOH (mass ratio)	2.5	2.5	2.5
AAS/FA (mass ratio)	0.4818	0.4687	0.4141
Heat curing	60 °C, 24 h	60 °C, 24 h	60 °C, 24 h

All specimens were heat-cured at 60 °C for 24 h. This regime was not intended to represent a universal optimum for all Class F fly ash geopolymers; rather, it was chosen as a practical curing condition for the material system adopted in this study. Previous studies have shown that heat curing for about 24 h is commonly used for fly ash-based geopolymer concrete, and that 60 °C can provide effective early strength development, while higher temperatures mainly accelerate the reaction. In the experimental basis underlying the present mixtures, curing at 60 °C for 24 h produced strength levels close to those obtained at 80 °C and 100 °C after the same curing duration, with lower energy demand. For this reason, 60 °C for 24 h was selected for all specimens in the present study. The granulometric distributions of the coarse and fine aggregates used in this study are presented graphically in Figure 1. The coarse aggregate grading was selected to satisfy ASTM C33, while the fine aggregate grading was determined based on sieve analysis in accordance with ASTM C136.

As shown in Table 4, all mixtures were designed as normal-density geopolymer concretes with the same target fresh unit weight. The principal difference among the three mixtures was their compressive strength, which increased from G30 to G50. Therefore, the variation in bond behavior observed in this study is interpreted mainly as a consequence of matrix-strength development rather than of density variation.

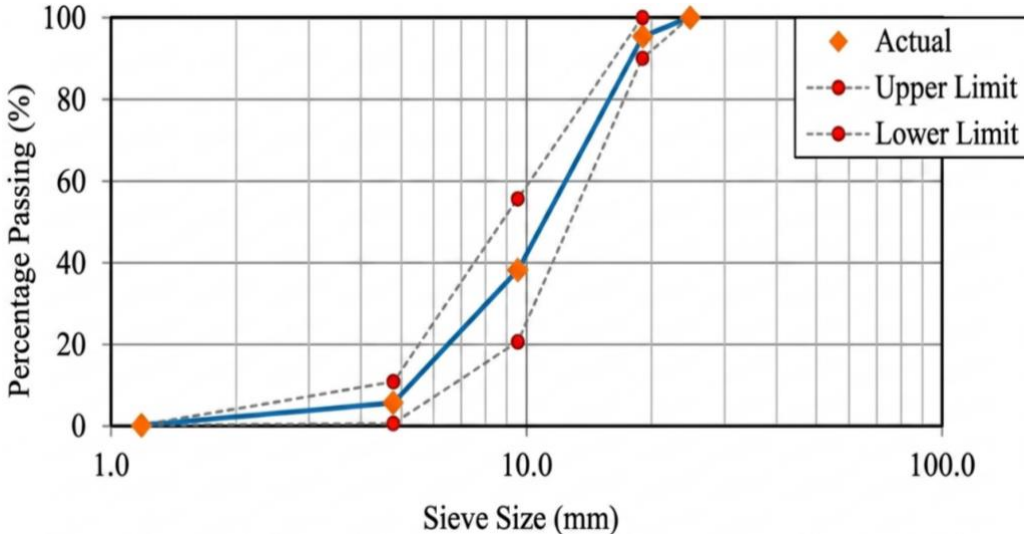

(a)

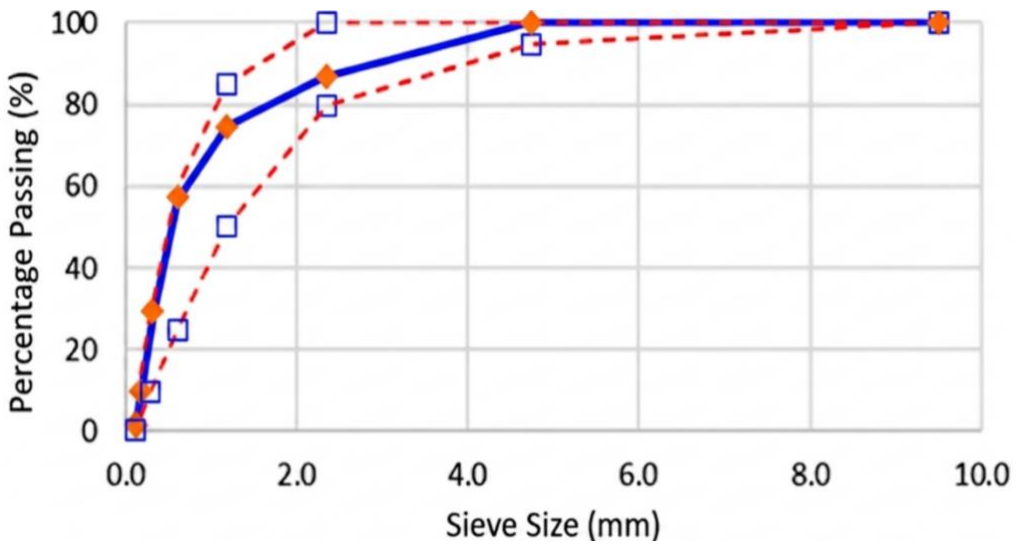

(b)

Fig. 1. Aggregate granulometry: (a) coarse aggregate grading; (b) fine aggregate grading

Table 4. Basic physical and mechanical characteristics of the tested GPC mixtures

Mixture	Target fresh unit weight, γ_t (kg/m^3)	Reference normal-density range, ρ_{ref} (kg/m^3)	Mean compressive strength, f_{cm} (MPa)	Characteristic compressive strength, (f'_c) (MPa)
G30	2400	2360 ± 60	39.46	31.67
G40	2400	2360 ± 60	49.86	40.46
G50	2400	2360 ± 60	59.81	52.06

Note: The target fresh unit weight was fixed at 2400 kg/m^3 for all mixtures. A typical hardened density of approximately 2360 ± 60 kg/m^3 has been reported for fly ash-based geopolymer concrete with granite aggregates after heat curing at 60 °C for 24 h. Direct hardened-density measurements of the present batches were not reported; therefore, the density information is presented here as a reference normal-density range rather than as measured values.

2.2. Specimen Details

Pull-out specimens were prepared in accordance with the specimen concept recommended in EN 10080:1995. The concrete specimen was a cube with a side length of 200 mm. A single deformed reinforcing bar was embedded concentrically in the cube. The reinforcing bar had a nominal diameter of 22 mm (ϕ22). The bar grade was CB400V steel.

Table 5. Pull-out specimen geometry and test matrix

Item	Value / description
Concrete specimen	200 × 200 × 200 mm cube
Reinforcing bar	Deformed bar, ϕ22 mm, grade CB400V
Bonded length, lb	5db = 110 mm
Debonding method	Plastic sleeve on the non-test portion of the embedded bar
Number of specimens	18 total
Specimens per mixture	6 per mixture (G30, G40, G50)
Reference procedure	EN 10080:1995 specimen concept

The bonded (anchorage) length was set to five times the bar diameter. The bonded length was therefore 110 mm. The remaining embedded bar length inside the concrete was intentionally deboned using a plastic sleeve. This arrangement ensured that bond stresses were mobilized only over the target bonded zone. The protruding bar length above the concrete surface was reserved for gripping and for slip measurement. A total of 18 pull-out specimens were cast. Six specimens

were prepared for each geopolymer mixture (G30, G40, and G50). The corresponding compressive strength levels used in the bond tests were within the intended range for the three mixtures (Table 5).

Fig. 2. Schematic of pull-out specimen

2.3. Test Setup and Instrumentation

Pull-out tests were performed using a direct tension configuration consistent with the EN 10080:1995 specimen concept. The concrete cube was positioned on a rigid steel support plate. A circular hole was provided at the center of the plate. The hole diameter was set to 2db. Fig. 3 presents a schematic diagram of the pull-out specimen used in the bond-strength test. The specimen consisted of a 200 × 200 × 200 mm concrete cube with a centrally embedded ϕ22 deformed steel bar, in which the bonded length was limited to 5db (110 mm) and the remaining embedded portion was debonded by means of a plastic sleeve. The figure is intended to provide a clear representation of the specimen geometry and the main parameters governing the test.

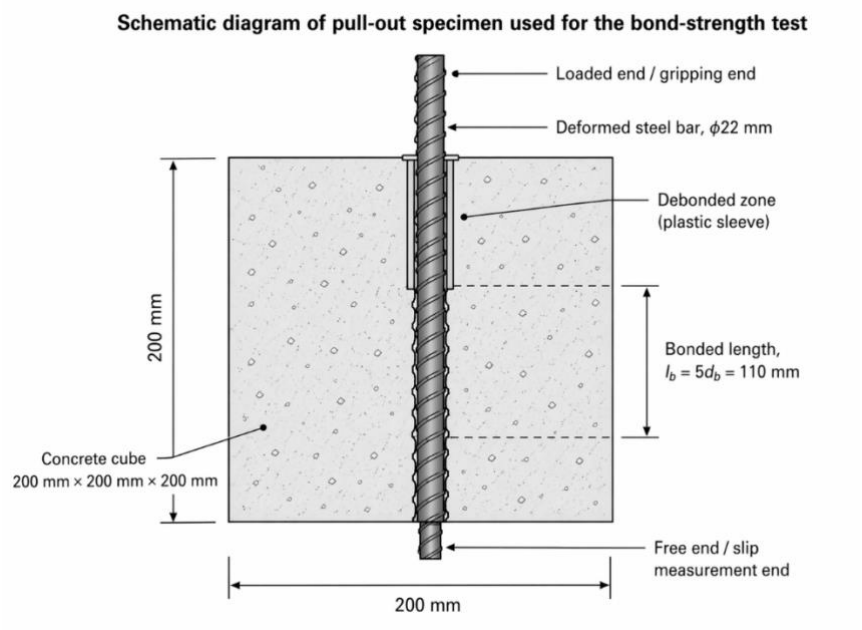

Fig. 3. Schematic diagram of the pull-out specimen used for the bond-strength test

Fig. 4. Test setup and instrumentation

The reinforcing bar passed through the hole and was clamped by the testing machine grips. The tensile load was applied at the longer protruding end of the bar. The slip was measured at the shorter end of the specimen, which represents the loaded-end slip definition adopted in the test procedure. During testing, the concrete cube was placed on a rigid steel support plate. A circular hole was provided at the center of the plate to allow the reinforcing bar to pass through without bearing directly on the plate. The hole diameter was $2d_b$. The loaded end of the protruding reinforcing bar was clamped by the grips of the testing machine, while the concrete specimen remained supported on the steel plate. Therefore, when tensile load was applied by the machine, the force was transferred to the embedded bar and bond stresses were mobilized along the bonded length inside the concrete. The slip was measured at the free end of the specimen, corresponding to the shorter protruding end of the reinforcing bar below the concrete cube. The loading rate was defined as $V = 0.56\ d^2$. For d_b=22 mm, the corresponding rate was V=271. The applied load was recorded continuously by the testing machine.

2.4. Data Processing

The test data consisted of the applied tensile force P and the measured bar slip s. The bond stress was computed by assuming uniform bond stress along the bonded length. The bond stress τ was calculated as:

$$\tau(s) = \frac{P(s)}{A_b} = \frac{P(s)}{\pi d_b l_b} \tag{1}$$

where A_b is the bonded surface area of the bar, d_b=22 mm is the bar diameter, and l_b=5d_b =110 mm is the bonded length. The τ-s curve was obtained by pairing τ(s) with the measured slip s throughout the loading history.

A characteristic bond stress was extracted at s = 1 mm. This value was used because, for normal concrete, the characteristic slip s_1 is approximately 1 mm in the MC90 bond model. In this study, the average bond force F_b recorded at s = 1 mm was used to compute the corresponding bond stress. The peak bond stress τ_{max} was taken as the maximum value on the measured τ–s curve. The slip at peak, $s(\tau_{max})$, was recorded for each specimen. For comparison with conventional OPC-based design, the reference peak bond stress in "good" bond conditions was computed using the CEB-FIP MC90 expression:

$$\tau_{\max,MC90} = 2\sqrt{f_{ck}} \tag{2}$$

where f_{ck} is the characteristic compressive strength.

3. Results and Discussion

3.1. Failure Modes

Two principal bond failure modes are commonly reported in pull-out–type tests. One mode is pull-out failure. The other mode is splitting failure. Bond deterioration progresses in stages. The first stage is the loss of chemical adhesion at the steel–concrete interface. The second stage is the formation of transverse microcracks in the surrounding concrete. The final stage is the development of radial stresses at the ribs. These radial stresses can exceed the tensile capacity of concrete and trigger splitting.

In the present test series, all specimens failed by concrete splitting in the bonded region. The concrete cube split into two parts along the bar line. The failure was sudden. The behavior was brittle. This observation is consistent with the failure pattern reported for the test specimens

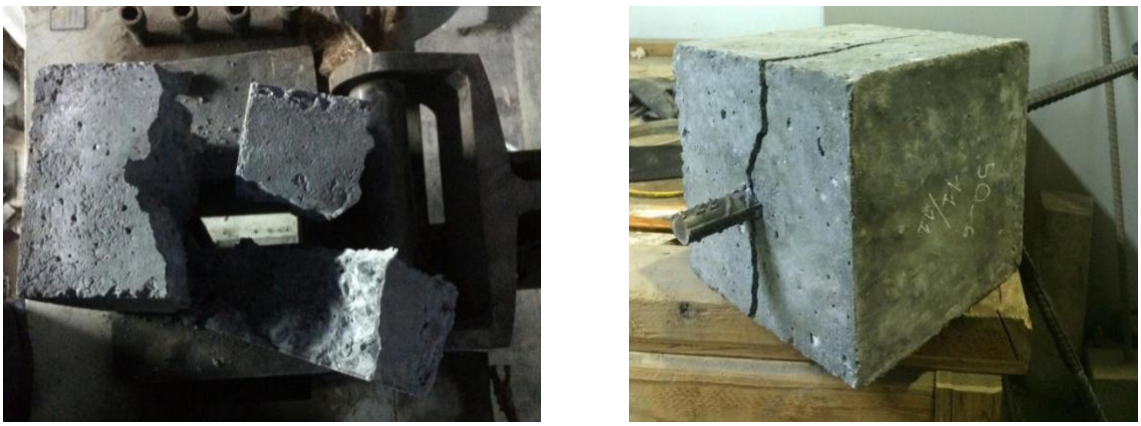

Fig. 5. Failure modes observed after testing

3.2. Bond Stress–Slip Response (τ–s Curves)

The bond stress–slip response was derived from the measured pull-out force–slip curves of the three mixtures. The response is expressed in terms of the average bond stress τ and the measured bar slip s. The τ–s curves show an initial ascending branch. This branch corresponds to the progressive loss of chemical adhesion and the mobilization of rib-bearing and frictional surfaces. The bond stress then approaches a peak value τ_{max}. The peak is reached after a limited amount of slip.

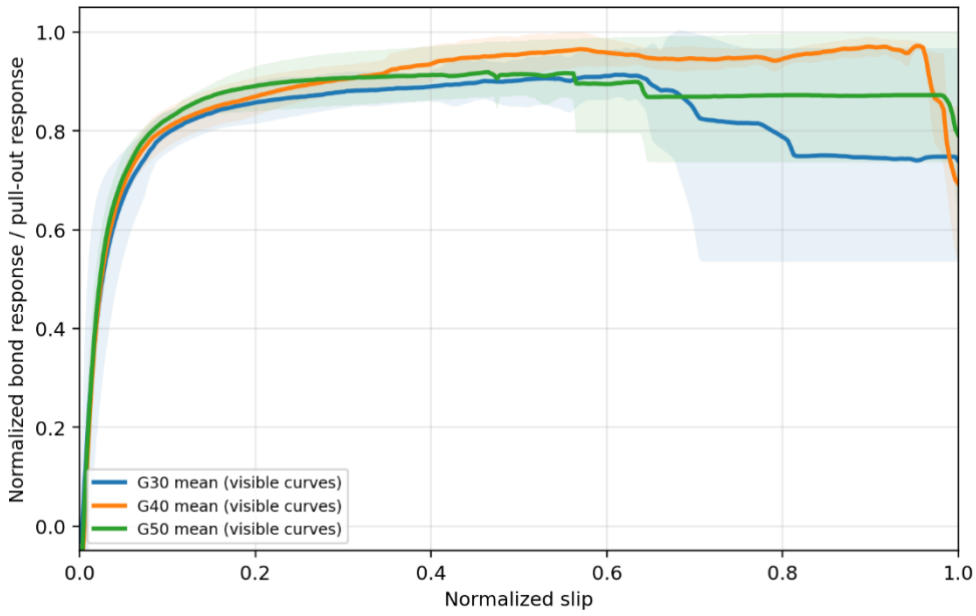

Fig. 6. Mean normalized bond stress–slip response curves of G30, G40, and G50 mixes

After the peak, the response softens. The softening is abrupt because the governing failure mode is concrete splitting. The post-peak branch, therefore, exhibits a steep drop in bond stress with increasing slip. A characteristic bond level was evaluated at s=1mm. This reference slip was adopted because it is commonly used in the MC90 bond model for ordinary concrete. The bond stress at this slip provides a consistent basis for comparing mixtures and for comparing fly ash GPC against OPC-based bond models.

3.3. Effect of Key Parameters

The test results clearly show that the bond response of the fly ash-based geopolymer concrete improved with increasing compressive strength. The average bond stress at a slip of 1 mm increased from 16.07 MPa for G30 to 16.69 MPa for G40 and 18.57 MPa for G50, while the corresponding compressive strengths increased from 31.67 MPa to 40.46 MPa and 52.06 MPa, respectively. This trend indicates that a higher concrete strength enhanced the resistance of the surrounding matrix against the local bearing stresses generated by the ribs of the deformed bar, thereby delaying the onset of longitudinal cracking and increasing the attainable bond level. Although the increase was not perfectly proportional to compressive strength, the overall tendency was consistent and confirms that the compressive strength of geopolymer concrete is an important parameter governing bar–concrete interaction in pull-out type bond tests.

The observed trend is in good agreement with previous studies on reinforced fly ash-based geopolymer concrete. Sarker reported that the bond strength of reinforcing steel embedded in fly ash-based geopolymer concrete was higher than that of comparable OPC concrete and that bond resistance increased with concrete strength [36]. More recently, Yuan et al. [27] also found that the ultimate bond strength of steel bars in unconfined fly ash-based geopolymer concrete increased with increasing concrete compressive strength. Taken together with the present results, these findings suggest that the beneficial effect of compressive strength on bond is not limited to OPC concrete but is also characteristic of fly ash-based geopolymer systems. This may be attributed to the denser geopolymer matrix and its stronger resistance to local splitting stresses around the ribs, which improve stress transfer at the steel–concrete interface.

At the same time, the present tests showed that all specimens failed by splitting rather than by a pure pull-out mechanism. This indicates that the ultimate bond resistance was governed primarily by the tensile capacity of the surrounding concrete cover and not solely by the adhesion and mechanical interlock at the steel surface. Once the radial stresses induced by rib bearing exceeded the splitting resistance of the unconfined concrete, longitudinal cracks propagated rapidly along the embedded bar, leading to a sudden post-peak degradation in bond stress. This interpretation is consistent with the failure patterns reported in previous bond studies on geopolymer concrete, where splitting has been identified as the dominant failure mode under limited confinement. Therefore, the present increase in bond stress with compressive strength should be understood as an increase in splitting-controlled bond capacity rather than as evidence of a fundamental change in the failure mechanism.

3.4. Comparison with OPC-Based Models

A comparison with previous studies indicates that the present bond levels are realistic for fly ash-based geopolymer concrete and are not anomalously high. The measured bond stresses exceeded the MC90 reference values for good bond conditions by approximately 13–43%, depending on the concrete strength level. This result supports the view that bond models originally developed for OPC concrete may be conservative when applied to geopolymer concrete. A similar conclusion was drawn by Sarker [36], who showed that the bond strength of reinforcing steel in fly ash-based geopolymer concrete was higher than that in comparable OPC concrete and suggested that existing OPC-based expressions could be conservatively used for geopolymer concrete. Recent studies and reviews have also emphasized that bond behavior in geopolymer concrete is often at least comparable to, and in many cases better than, that of OPC systems, particularly when the geopolymer matrix exhibits high splitting tensile resistance and a dense interfacial structure [25,27,32].

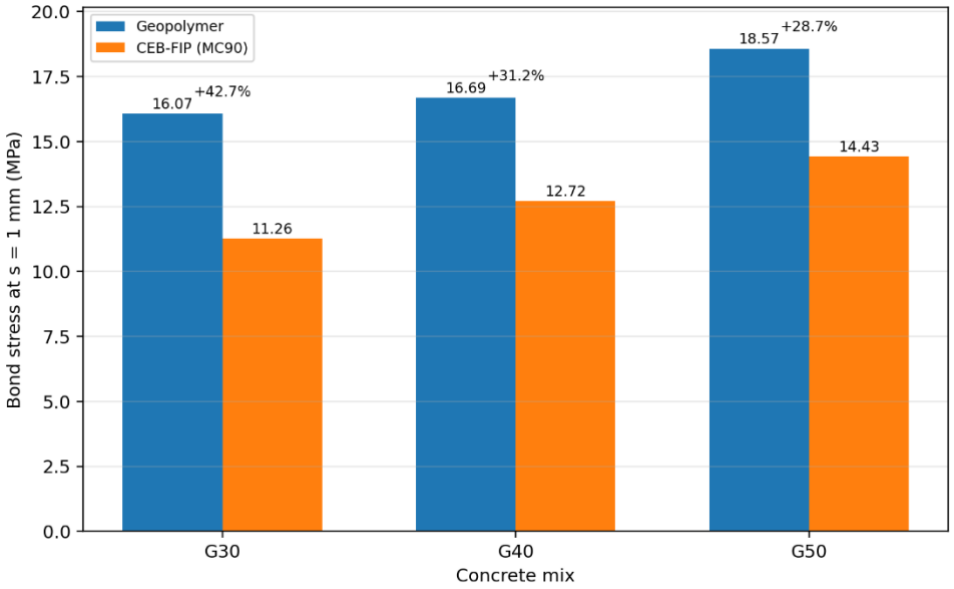

Fig. 7. Bond stress versus compressive strength for geopolymer concrete compared with the CEB-FIP Model Code 1990 (MC90)

The higher bond performance of geopolymer concrete reported in the literature has been linked to microstructural features of the geopolymer matrix. Compared with OPC concrete, fly ash-based geopolymer concrete may develop a denser binder phase and a more compact interfacial transition zone, which enhance the transfer of shear and bearing stresses from the ribs of the bar to the surrounding matrix. However, the present results also show that a higher bond stress does not necessarily imply a more ductile bond response. Because all specimens failed by splitting, the bond capacity remained strongly dependent on the tensile resistance of the concrete cover and on the confinement condition. In this sense, the present results are consistent with the broader literature: geopolymer concrete can exhibit high bond resistance, but the governing failure mode may still be brittle when confinement is insufficient.

From a design perspective, the present results suggest that MC90 provides a conservative estimate of bond strength for the tested fly ash-based geopolymer concrete, and this conservatism explains why the development lengths derived from the experimental bond stresses are shorter than those obtained from the code-based prediction. Nevertheless, this implication should be interpreted with caution. The present study used a single bar diameter, a fixed bonded length, and unconfined pull-out specimens that consistently failed by splitting. Therefore, the reduction in calculated development length should not be generalized to all geopolymer concretes or all anchorage conditions. Rather, the main implication of the present results is that fly ash-based geopolymer concrete may warrant a dedicated calibration of bond and development-length expressions, especially for cases where the cover, confinement, and curing regime are similar to those adopted in the present experimental program.

4. Model Development and Design Implications

The significance of the present model development lies in converting the experimental bond results into a form that is directly usable for structural analysis and preliminary design. Experimental bond stress–slip curves provide important physical insight, but by themselves they remain specific to the tested materials, geometry, and curing regime. A calibrated bond model is therefore needed to represent the measured response in a compact analytical form, so that it can be used to estimate bond resistance, compare fly ash-based geopolymer concrete with OPC-based assumptions, and discuss practical implications for anchorage and development length. In this study, the objective is not to propose a fully general design law for all geopolymer concretes, but rather to provide a simple calibration of an established OPC-based model that captures the main features of the measured bond response of the investigated fly ash GPC.

4.1. Baseline Model and Calibration Objective

This study adopts the CEB–FIP MC90 bond framework as a baseline model. The baseline peak bond stress for good bond conditions is computed as $\tau_{\max,MC90} = 2\sqrt{f_{ck}}$. The experimental bond stress is evaluated from the pull-out force and the bonded surface area. The bond stress at s=1 mm is selected as a characteristic value because MC90 commonly uses s1≈1 mm for ordinary concrete.

The test results show that the bond stress at s=1 mm for fly ash GPC is higher than the MC90 prediction. The manuscript-level summary indicates an increase of about 13–43% relative to MC90. This systematic bias motivates a simple calibration factor that preserves the MC90 functional form and improves agreement for fly ash GPC.

4.2. Proposed Calibrated Bond Level for Fly Ash GPC

A practical calibration is introduced through three parameters (a,b,k). The parameter a scale the bond stress level. The parameter b scales the slip axis. The parameter k scales the post-peak level. The calibrated law is written in a compact form as:

$$\tau_{GPC}(s) = a\tau_{MC90}\frac{s}{b} \tag{3}$$

and

$$\tau_{GPC,post}(s) = k\tau_{GPC}(s) \quad \textit{for the descending branch} \tag{4}$$

The available dataset provides robust information on bond stress levels at s=1 mm and at peak. The dataset does not provide sufficient landmark points to uniquely re-fit the full curve shape for each mixture. Therefore, the calibration focuses on the stress level. The slip and post-peak shape are preserved. This choice is consistent with using MC90 as a baseline and applying a design-friendly correction.

Table 6. Proposed calibration parameters and fitting errors

Parameter	Meaning	Value
a	stress scaling factor for MC90 (τ level)	1.34
b	slip scaling factor (shape preservation)	1.00
k	post-peak / residual scaling factor (shape preservation)	1.00
Fitting errors (for τ at s = 1 mm across mixes)		
Metric		Value
MAE (MPa)		0.71
RMSE (MPa)		0.75
MAPE (%)		4.18

The proposed calibration parameters and fitting errors are summarized in Table 6. The value a=1.34 represents the average amplification of the bond level relative to MC90 at s=1 mm over the investigated mixtures. The parameters b and k are set to 1.00 to preserve the MC90 curve shape.

4.3. Design Implications for Development Length And Lap Splice

Bond-controlled anchorage and lap splice lengths are inversely related to the effective bond stress that can be mobilized along the bar. This relationship provides a direct link between the calibrated bond model and practical detailing. A first-order implication can be expressed using a normalized ratio:

$$\frac{l_{d,GPC}}{l_{d,OPC}} \approx \frac{\tau_{OPC}}{\tau_{GPC}} \tag{5}$$

If the OPC reference is MC90 and the GPC level is determined from the measured τ at s=1 mm, the ratio can be evaluated for each mixture. The results are reported in Table 7. The computed ratios range from about 0.70 to 0.78 for the investigated strength levels.

Table 7. Normalized comparison of development length (MC90 vs calibrated for GPC)

Mix	f'c (MPa)	τ_GPC,mean at s=1 mm (MPa)	τ_MC90,max (MPa)	τ_GPC / τ_MC90	l_d,GPC / l_d,OPC
G_30	31.67	16.07	11.26	1.43	0.70
G_40	40.46	16.69	12.72	1.31	0.76
G_50	52.06	18.57	14.43	1.29	0.78

The trend of $l_{d,GPC}/l_{d,OPC}$ with compressive strength is illustrated in Figure 8. The ratio increases slightly as fc′ increases in the investigated range. This occurs because the relative exceedance of GPC over MC90 decreases with increasing strength in the present dataset.

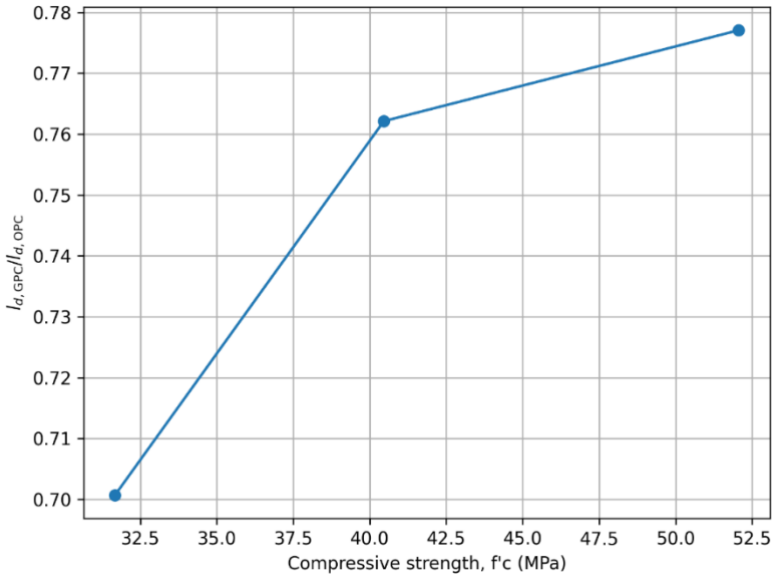

Fig. 8. Effect of compressive strength on the development-length reduction factor for fly ash geopolymer concrete

The above implications must be interpreted together with the observed failure mechanism. All pull-out specimens failed by splitting. Splitting is sensitive to concrete cover and confinement. The proposed reduction in development or splice length is therefore applicable only when the cover and confinement are comparable to those of the tested configuration. A conservative design approach can still use MC90 directly because MC90 provides a lower-bound estimate for the investigated fly ash GPC system at the reference slip level.

From an engineering perspective, the value of this calibration is that it allows the experimental findings to be interpreted in a design-oriented manner. Instead of treating the measured bond behavior only as an isolated set of test results, the calibrated model provides a practical means of quantifying how much the bond level of the investigated fly ash GPC differs from that assumed in the conventional MC90 formulation. This, in turn, enables a first-order assessment of development-length demand and shows how existing OPC-based provisions may be conservatively adapted for reinforced fly ash-based geopolymer concrete under conditions comparable to those examined in this study.

5. Conclusions

This paper investigated the bond performance of deformed steel bars in fly ash–based geopolymer concrete (GPC) using pull-out tests with a 22 mm bar and a bonded length of 5db (110 mm). The following conclusions are drawn.

- All tested specimens failed by concrete splitting in the bonded region. The failure was sudden and brittle.

- The measured bond response exhibited a rapid post-peak drop. This trend is consistent with splitting-controlled behavior rather than a stable pull-out mechanism.
- The bond level of fly ash GPC at the reference slip s = 1mm was higher than the OPC-based MC90 prediction for good bond conditions. The exceedance ranged from about 13% to 43% for the investigated mixtures.
- A simple calibration that preserves the MC90 curve shape and scales the stress level was proposed. The recommended parameters are a=1.34, b=1.00, and k=1.00.
- The calibration errors for τ at s=1 mm are low (MAE ≈ 0.71 MPa, RMSE ≈ 0.75 MPa, and MAPE ≈ 4.18%).
- The higher bond level implies shorter anchorage demand in a first-order sense. The normalized ratio ld,GPC/ld,OPC derived from the experimental bond level is about 0.70–0.78 for the investigated strength range.
- The above design implication must be interpreted together with the observed splitting failure. Bond capacity is sensitive to cover and confinement. Therefore, any reduction of development or splice length should be adopted only when detailing conditions are comparable to those in the tests.
- The main significance of the proposed model is that it bridges the gap between experimental bond characterization and practical structural application by enabling a first-order calibration of development-length demand for reinforced fly ash-based geopolymer concrete.

References

[1] Nga NTT, Minh TQ, Thong PQ, Thuc NV. An experimental study on the influence of fine and coarse aggregates on the strength of polyurethane concrete for highway maintenance. Matéria (Rio de Janeiro). 2025. https://doi.org/10.1590/1517-7076-rmat-2025-0269

[2] Ngo TV, Le TK, Nguyen NTC, Le BH, Tran MQ. Study on flexural behavior of ultra-high-performance concrete beams using finely ground rice husk ash. J Mater Eng Struct. 2024.

[3] Yaswanth KK, Kumar GP, Vani VS, et al. Feasibility study of novel Bengal Gram Husk Ash as a supplementary cementitious material: mechanical, durabilty and microstructural assessments. Multiscale Multidiscip Model Exp Des. 2025. https://doi.org/10.1007/s41939-024-00629-7

[4] Tran VH, Tran M. Mechanical properties and structural behavior of optimized fly ash-based geopolymer concrete: Experimental and numerical investigation. Case Studies in Construction Materials. 2026. https://doi.org/10.1016/j.cscm.2026.e06012

[5] Adnan M, Anas M. Geopolymer concrete as a sustainable alternative to OPC. J Umm Al-Qura Univ Eng Archit. 2025. https://doi.org/10.1007/s43995-025-00155-8

[6] Tamoor M, Zhang C. Sustainable geopolymer concrete: A comprehensive lifecycle and performance assessment. Next Research. 2025. https://doi.org/10.1016/j.nexres.2025.100956

[7] Peng C, Mao Y, Li S, Xing Y, Du Y, Shi C. Research progress on the structural performance of reinforced geopolymer concrete columns. J Build Eng. 2025. https://doi.org/10.1016/j.jobe.2025.113805

[8] Yaswanth KK, Revathy J, Gajalakshmi P. Influence of copper slag on Mechanical, durability and microstructural properties of GGBS and RHA blended strain hardening geopolymer composites. Constr Build Mater. 2022. https://doi.org/10.1016/j.conbuildmat.2022.128042

[9] Yaswanth KK, Begum S, Kumar GP, et al. Development of lightweight high-strength engineered geopolymer composites using slag waste and vermiculite powder: mechanical, durability and microstructural assessments. Emergent Mater. 2025.

[10] Van TN, Thi Thu NN, Le BH, Tran Quang M, Hoang VH, Tran BH. Development of Green Ultra High Performance Concrete with low cement content using mineral powders and nano-silica extracted from rice husk ash. Case Studies in Construction Materials. 2025. https://doi.org/10.1016/j.cscm.2025.e05537

[11] Nguyen TTN, Doan LP, Nguyen TH, Minh TQ. Influence of Graphene Oxide (GO) and Fly Ash (FA) on the workability and mechanical properties of self-compacting concrete. J Sci Transp Technol. 2025.

[12] Nga NTT, et al. Effects of Fly Ash and Graphene Oxide in Cement Mortar Considering the Local Recycled Material Context. Appl Sci. 2024.

[13] Yang H, Liu L, Yang W, Liu H, Ahmad W, Ahmad A, et al. A comprehensive overview of geopolymer composites: A bibliometric analysis and literature review. Case Studies in Construction Materials. 2022. https://doi.org/10.1016/j.cscm.2021.e00830

[14] Khasawneh MA. Geopolymer concrete in construction projects: a review. Low-carbon Mater Green Constr. 2025. https://doi.org/10.1007/s44290-025-00281-1

[15] Vembu S, Raman P, Ammasi AK. A Comprehensive Review on the Factors Affecting Bond Strength in Concrete. Buildings. 2023.
[16] Wang Z, Su L, Mai Z, et al. Bond durability between geopolymer-based CFRP composite and OPC concrete substrate in seawater environments. J Build Eng. 2024. https://doi.org/10.1016/j.jobe.2024.109817
[17] He X, Zhang W, Liu Y, Zhang Y, Yu Y, Niu M, et al. Study on the Interfacial Bonding Behavior of OPC-GGBS-SAC Composite Repair Materials. Buildings. 2025. https://doi.org/10.3390/buildings15224124
[18] Bai L, Zhao Q, Zhao J, Yin L, Zhao Y. Experimental Study on Bond and Force Transmission Properties of Steel Reinforcement in Non-Contact Lap Splice Encased in Calcium Sulphoaluminate Cement-Based Micro Steel Fiber Concrete. Buildings. 2024. https://doi.org/10.3390/buildings14092716
[19] Krishnaveni S, Rajendran S. Experimental studies on bond behaviour of steel rebar with different rib patterns in concrete. J Build Eng. 2024. https://doi.org/10.1016/j.jobe.2024.110157
[20] Dey A, Bado MF, Kaklauskas G. Validation of reinforced concrete bond stress-slip models through an analytical strain distribution comparison. Mater Struct. 2022. https://doi.org/10.1617/s11527-022-02071-y
[21] Bencardino F, Condello A. SRG/SRP-concrete bond-slip laws for externally strengthened RC beams. Compos Struct. 2015. https://doi.org/10.1016/j.compstruct.2015.06.068
[22] Amin MN, Iqbal M, Althoey F, Khan K, Faraz MI, Qadir MG, et al. Investigating the Bond Strength of FRP Rebars in Concrete under High Temperature Using Gene-Expression Programming Model. Polymers. 2022. https://doi.org/10.3390/polym14152992
[23] Tran TT, Pham HM, Hao H. Rectangular Stress-block Parameters for Fly-ash and Slag Based Geopolymer Concrete. Structures. 2019. https://doi.org/10.1016/j.istruc.2019.01.006
[24] Alzeebaree R. Bond Strength and Fracture Toughness of Alkali Activated Self-Compacting Concrete Incorporating Metakaolin or Nanosilica. Sustainability. 2022. https://doi.org/10.3390/su14116798
[25] Cui Y, Ai W, Tekle BH, et al. State of the art review on the production and bond behaviour of reinforced geopolymer concrete. Low-carbon Mater Green Constr. 2023. https://doi.org/10.1007/s44242-023-00027-1
[26] Zhang P, Wang K, Li Q, Wang J, Ling Y. Fabrication and engineering properties of concretes based on geopolymers/alkali-activated binders - A review. J Clean Prod. 2020. https://doi.org/10.1016/j.jclepro.2020.120896
[27] Yuan J, Xiao J, Huang D. Experimental research on bond behavior of high-strength reinforcement in unconfined fly ash-based geopolymer concrete. Case Studies in Construction Materials. 2025. https://doi.org/10.2139/ssrn.5217139
[28] Zheng Y, Xiao Y. A comparative study on strength, bond-slip performance and microstructure of geopolymer/ordinary recycled brick aggregate concrete. Constr Build Mater. 2023. https://doi.org/10.1016/j.conbuildmat.2022.130257
[29] Zhang X, Gong J, Lv Y, Zheng Q, Li C. Experimental study on confinement-dependent mechanical behavior and failure criteria of high-strength geopolymer concrete. Constr Build Mater. 2025. https://doi.org/10.2139/ssrn.5351783
[30] Abadel AA. Structural Performance of Strengthening of High-Performance Geopolymer Concrete Columns Utilizing Different Confinement Materials: Experimental and Numerical Study. Buildings. 2023. https://doi.org/10.3390/buildings13071709
[31] Li N, Shi C, Zhang Z, Wang H, Liu Y. A review on mixture design methods for geopolymer concrete. Compos B Eng. 2019. https://doi.org/10.1016/j.compositesb.2019.107490
[32] Cui Y, Qu S, Bao J, Zhang P. Bond Performance of Steel Bar and Fly Ash-Based Geopolymer Concrete in Beam End Tests. Polymers. 2022. https://doi.org/10.3390/polym14102012
[33] Azunna SU, Aziz FNAA, Rashid RSM. Review on structural characteristics of reinforced geopolymer concrete. Progress in Engineering Science. 2025. https://doi.org/10.1016/j.pes.2025.100083
[34] Tran VH, Dao VD, Nguyen NL. Investigation on the adhesion bonding between fly ash based geopolymer concrete and reinforcement. Tap Chi GTVT. 2013.
[35] Tran VH. Research on the composition and mechanical properties of fly ash geopolymer concrete and its application in bridge and tunnel structures [PhD thesis]. University of Transport and Communications; 2017.
[36] Sarker PK. Bond strength of reinforcing steel embedded in fly ash-based geopolymer concrete. Mater Struct. 2011. https://doi.org/10.1617/s11527-010-9683-8